Published in final edited form as:

Cancer Res. 2019 August 01; 79(15): 3928–3939. doi:10.1158/0008-5472.CAN-19-0056.

Deletion of calcineurin promotes a pro-tumorigenic fibroblast phenotype

Allyson Lieberman[1,2], **Richard Barrett**[2], **Jaewon Kim**[1], **Kathy L. Zhang**[1], **Diana Avery**[2], **James Monslow**[2], **Hyunsoo Kim**[3], **Bang-Jin Kim**[1], **Ellen Pure**[2], **Sandra Ryeom**[1]

[1]Department of Cancer Biology, Perelman School of Medicine at the University of Pennsylvania, Philadelphia, PA

[2]Department of Biomedical Sciences, University of Pennsylvania School of Veterinary Medicine, Philadelphia, PA

[3]Department of Pathology and Laboratory Medicine, Perelman School of Medicine at the University of Pennsylvania, Philadelphia, PA

Abstract

Fibroblast activation is a crucial step in tumor growth and metastatic progression. Activated fibroblasts remodel the extracellular matrix (ECM) in primary tumor and metastatic microenvironments, exerting both pro- and anti-tumorigenic effects. However, the intrinsic mechanisms that regulate the activation of fibroblasts are not well-defined. The signaling axis comprising the calcium-activated Ser/Thr phosphatase calcineurin (CN), and its downstream target nuclear factor of activated T cells (NFAT), has been implicated in endothelial (EC) and immune cell activation, but its role in fibroblasts is not known. Here, we demonstrate that deletion of CN in fibroblasts *in vitro* altered fibroblast morphology and function consistent with an activated phenotype relative to wild-type fibroblasts. CN-null fibroblasts had a greater migratory capacity, increased collagen secretion and remodeling, and promoted more robust EC activation in vitro. ECM generated by CN-null fibroblasts contained more collagen with greater alignment of fibrillar collagen compared to wild-type fibroblast-derived matrix. These differences in matrix composition and organization imposed distinct changes in morphology and cytoskeletal architecture of both fibroblasts and tumor cells. Consistent with this in vitro phenotype, mice with stromal CN deletion had a greater incidence and larger lung metastases. Our data suggest that CN signaling contributes to the maintenance of fibroblast homeostasis, and that loss of CN is sufficient to promote fibroblast activation.

Keywords

calcineurin/NFAT; fibroblast activation; metastasis; extracellular matrix

Corresponding authors: Ellen Puré, Department of Biomedical Sciences, University of Pennsylvania, Philadelphia, PA. Phone: (215)-573-9406 epure@upenn.edu. Sandra Ryeom, Department of Cancer Biology, Perelman School of Medicine at the University of Pennsylvania, Philadelphia, PA. Phone: (215)-573-5857. sryeom@upenn.edu.

Conflicts of interest: The authors declare no potential conflicts of interest.

Introduction

The tumor microenvironment (TME) consists of multiple cell types, including endothelial (EC), immune, and stromal cells (1) and is an appealing target for cancer. Fibroblasts are cells of mesenchymal origin important in normal and diseased stroma. Resident fibroblasts orchestrate and maintain extracellular matrix (ECM) in normal tissues, but matrix remodeling present in both physiologic and pathologic processes such as wound healing, fibrosis, and cancer require fibroblast activation (2). Studies indicate that normal tissues are resistant to tumor cell colonization due in part to fibroblast homeostasis, and that fibroblast activation is required for primary tumor progression and metastatic colonization (2,3). While stimuli that promote fibroblast activation have been identified, the cell-intrinsic mechanisms underlying the transition from quiescent to activated fibroblasts, or the “stromagenic switch,” are poorly understood.

Widely used markers of activated fibroblasts include fibroblast activation protein (FAP) (4,5) and the myofibroblast marker alpha-smooth muscle actin (αSMA) (6). These markers delineate heterogeneous populations of activated fibroblasts with unique context- and tissue-dependent gene expression profiles (7). Activated fibroblasts increase their migration and contractility, secrete and remodel ECM, and produce cytokines and growth factors that affect cells in the microenvironment. Stimuli responsible for fibroblast activation include changes in substratum mechanical stiffness, composition and architecture of the ECM, growth factors such as TGFβ or PDGF and cellular stress such as hypoxia or ROS (8).

While many activating stimuli of fibroblasts and their downstream mediators are well-defined, less is known about cell-intrinsic pathways required for homeostasis in resident un-activated fibroblasts. It is evident that quiescence is not simply a default state but requires active maintenance (9). The calcineurin (CN)/nuclear factor of activated T cells (NFAT) signaling pathway was originally identified in T cells and has been shown by us and others to play key roles in other cells, including EC activation and tumor angiogenesis (10-12). CN is a calcium-regulated serine-threonine phosphatase with a catalytic (CNA) and a regulatory (CNB) subunit (13). Its best-known substrates are the NFAT family of transcription factors, that translocate to the nucleus after CN dephosphorylation transactivating tissue-specific genes. We previously demonstrated that the CN/NFAT pathway mediates EC activation downstream of VEGF, and that pharmacologic or genetic disruption of CN signaling affects primary tumor growth and metastatic progression (10-12). Studies have shown both pro- and anti-fibrotic effects of CN in fibroblasts (37-45), however, the role of CN in fibroblasts in the TME has not been extensively investigated.

As the CN/NFAT pathway regulates the function of many cells in the TME (14), we examined CN signaling in lung fibroblasts and assessed the impact of fibroblast-specific deletion of CN on lung metastasis. Here we demonstrate that CN deletion in fibroblasts leads to an activated phenotype ie, increased proliferation, migration, and contractility compared to wild-type (WT) fibroblasts. Our studies show that ECM from $Cn^{-/-}$ fibroblasts contain greater and more linearly aligned fibrillar collagen, and that $Cn^{-/-}$ fibroblasts support more robust EC tube formation *in vitro*. Furthermore, stromal cell specific *Cn* deletion in mice leads to increased incidence and size of lung metastases in an experimental

metastasis model with two different tumor cell lines. Our findings implicate CN in maintaining fibroblast homeostasis and attenuating the pro-tumorigenic activity of fibroblasts in metastatic lesions.

Materials and Methods

Primary lung fibroblast isolation and culture

Fibroblasts were cultured in DMEM-F12 + L-glutamine/penn-strep with 10% FBS. Lungs from 3–5-week-old mice were dissociated in HBSS containing 5 mg/ml type II collagenase and 0.5 mg/ml deoxyribonuclease I (Worthington, #LS004176 and #LS002139) and passed through 100μm and 40μm filters to obtain single cell suspensions; fibroblasts were cultured for 1–2 hours at 37° C then non-adherent cells were washed off. Fibroblast identity was confirmed by immunostaining for vimentin (goat, Santa Cruz #sc-7557), CD45.2 (biotinylated mouse, BD Pharmingen #553771), and CD31 (rat, BD Pharmingen #553370, 1:100), followed by secondary antibody and streptavidin (Alexa Fluor 647 anti-goat IgG, Alexa Fluor 488 anti-rat IgG, Alexa Fluor 555 streptavidin, Invitrogen #A-21447, A-11006, Thermo Fisher #S-21381 respectively); fibroblasts were >99% vimentin-positive, <5% $CD45^+$ and $CD31^-$.

For soft collagen gel cultures, fibroblasts were plated on thick 1 mg/ml type I collagen gels; type I rat tail collagen (Corning #354236) was diluted in 10X PBS at 1 mg/ml and neutralized using 1 N NaOH per manufacturer's instructions. Collagen gels solidified for 1–3 hours then fibroblasts were plated onto gels and cultured for 48 hours before imaging.

Calcineurin deletion *in vitro*

To delete *CnB in vitro*, P1 $CnB^{fl/fl}$ fibroblasts were treated with 300 MOI AdCMV-Cre (U Iowa Viral Vector Core Facility) overnight in 1% serum followed by PBS wash then addition of culture media. P3 fibroblasts were used for experiments. Controls include WT fibroblasts treated with AdCre, $CnB^{fl/fl}$ fibroblasts treated with AdGFP, or $CnB^{fl/fl}$ fibroblasts without AdCre.

Proliferation assays

Fibroblasts were plated in gelatin-coated plates and serum-starved overnight. Day 0 counts were measured, then either 1% or 10% FBS + DMEM-F12 culture media added. On indicated days, triplicate wells were stained with trypan blue and counted on a hemocytometer. EdU proliferation assays were performed with Click-iT EdU Alexa Fluor 594 Imaging Kit (Invitrogen) according to manufacturer's instructions; fibroblasts were pulsed with 10 μM EdU for 16–18 hours before fixation and staining.

In vitro scratch wound healing assays and live-cell imaging

Scratch assays were performed as described (15). Confluent cells in 12 well plates were scratched using a P200 pipet tip, washed with PBS, and replaced with culture media. Two experimental replicates were imaged at 0, 2, 6, 12, 24, and 48 hours post-wounding using an inverted microscope, and two replicates were imaged every 15 minutes using a Nikon inverted microscope with a stage incubator for live cell imaging with replicates stained using

the SiR-Hoechst far-red kit (Spirochrome #CY-SC007), and cell tracking analyzed using Nikon NIS-Elements software. Experimental conditions were performed in triplicate.

Transwell migration and invasion assays

Transwell inserts of 6.5mm (24 well) and 12mm (12 well) with a pore size of 8μm (Corning) were used. 5×10^4 (6.5mm) or 7.5×10^4 (12mm) WT or *Cn*$^{-/-}$ fibroblasts were plated in inserts containing serum-free media in the upper chamber and 10% serum in the lower chamber. For migration assays, inserts were uncoated; for invasion assays, inserts were coated with 75μl 1mg/ml neutralized type I rat tail collagen for 1 hour before cell seeding. For invasion assays, uncoated transwells were used as positive controls; for migration and invasion assays, serum-free media was placed in the lower chamber as negative controls. 24 hours following plating, the upper chamber was wiped with a cotton swab to remove remaining cells, washed with PBS, fixed and stained with 0.5% crystal violet in 25% methanol solution for 15 minutes, washed in deionized water, and dried before imaging. Images were taken by tile-scanning using a Zeiss Axio Imager M2 upright microscope with Zen Pro software. Crystal violet-positive area was measured using ImageJ. Assays were performed in triplicate and experiments repeated three times.

2P-SHG imaging and analysis

Fibroblasts cultured on collagen and FDMs were imaged on a Leica SP8 multi-photon upright confocal microscope. Forward SHG signal was collected, and in non-cell-extracted cultures, autofluorescence in an adjacent channel identified cells and differentiated between SHG and non-SHG signal. 3–5 images per sample were taken for analysis and Z-stacks were performed to obtain maximum intensity projections throughout sample thickness. Images were processed using LAS AF software. Collagen fiber analysis was performed using CT-FIRE and CurveAlign software.

Collagen contraction/remodeling assays

Collagen gel contraction assays were performed as described (16). 5×10^5 fibroblasts were embedded in 500 μl of 1 mg/ml rat tail type I collagen solution (Corning) in 24 well plates. Collagen gels solidified for 1 hour before detachment and 1% FBS was added. Images were taken at 0, 6, 12, 24, 48, and 72 hours post-detachment. Collagen gel areas were measured using ImageJ software; each time point was normalized to empty wells. Assays were performed in triplicate.

Collagenase activity

To visualize collagenase activity, fibroblasts were cultured in chamber slides coated with gelatin or a thick type I collagen gel as described (200 μl/well). DQ™ type I collagen from bovine skin conjugated to fluorescein (Invitrogen, #D12060) or DQ™ gelatin from pig skin (Invitrogen, #D12054) was overlaid on cultures (25 μg/ml). After 24 hours, cultures were fixed using Prefer (Anatech Ltd) or 4% paraformaldehyde (PFA) in PBS (Affymetrix/USB) and mounted using Fluorogel II with DAPI. Images were acquired using a Zeiss Axio Imager M2 upright fluorescent microscope and processed with Zen Pro software.

Fibroblast-derived matrix (FDM) generation, extraction, and analysis

FDMs were generated as per Cukierman et al. (17). 5×10^5 (35mm dish), 2×10^5 (12 well plate), or 5×10^4 (35mm glass bottom dish) fibroblasts were plated onto gelatin-crosslinked dishes at 100% confluency. 75 μg/ml L-ascorbic acid (Sigma-Aldrich #A4544) was added to culture media and changed every other day for 8–10 days. Matrices were decellularized using 0.5% Triton X-100 and 20 mM NH_4OH in PBS and stabilized at 4°C overnight. For earlier time points, FDMs were generated in triplicate and matrices were decellularized following 3 and 5 days of ascorbic acid treatment.

To generate tumor cell-conditioned media, SR0144 lung tumor cells (provided by Dr. Carla Kim, Harvard University) were grown to 80% confluence, and culture media replaced with serum-free DMEM for 24 hours, collected and centrifuged before use. Media for unstimulated and tumor-conditioned FDMs had a final serum concentration of 2.5% and consisted of a 1:1 dilution of either tumor-conditioned media or serum-free DMEM with 5% and 75 μg/ml L-ascorbic acid.

Western blotting of cell lysates and FDMs

Cells were lysed in RIPA buffer followed by SDS-PAGE of lysates (3–10μg/sample), transfer onto nitrocellulose membranes, blocking in 5% non-fat dry milk in TBS-T (TBS + 0.1% Tween 20) and incubation with primary antibody diluted in blocking buffer at 4°C overnight (CNA, Abcam #ab3673; actin, Sigma #A2668). Blots were washed in TBS-T, and secondary antibody (anti-rabbit IgG HRP conjugate, Cell Signaling CST7074) was added for 1 h at RT. Bands were visualized using enhanced chemiluminescence reagent (100 mM Tris pH 8.6, 0.2 mM p-coumaric acid, 1.25 mM luminol, 2.6 mM).

Imaging analysis of cells on FDMs

WT or $Cn^{-/-}$ fibroblasts or MH6449 PDAC cells (10^4) were plated in 35mm wells with WT or $Cn^{-/-}$ FDMs for 16 h before fixing with 4% PFA in PBS. Wells were blocked with 5% normal goat serum, 1% BSA, and 0.001% thimerosal in PBS, followed by Fc receptor blocking for 20 minutes (BD Pharmingen #553141). Primary antibodies were incubated in blocking buffer at 4°C overnight (paxillin, BD Biosciences #612405), and secondary antibodies were incubated in 1% BSA for 1 hour. Following secondary antibody incubation (Invitrogen #A-11032), Alexa Fluor 488-conjugated phalloidin (Cell Signaling Technologies, #8878S) was added before mounting with Fluorogel II with DAPI. Confocal imaging was performed on a Leica TCS SP5 laser scanning confocal microscope and processed using LAS AF software.

For live cell imaging, WT and $Cn^{-/-}$ FDMs were generated in 12 well plates and decellularized. 5×10^4 YFP^+ MH6449 PDAC cells or 1×10^5 GFP^+ primary lung ECs were plated onto decellularized matrices, and cell movement tracked for 24 hours. Individual cell tracking and velocity/direction analysis were performed using Nikon NIS-Elements software.

EC co-culture assays and angiogenic secretome analysis

Primary GFP$^+$ lung ECs were isolated and cultured (18). On day 0, 2.5×10^5 fibroblasts and ECs were mixed 1:1 and embedded in growth factor reduced basement membrane extract (BME, Trevigen #3533–001-02) in 35mm glass bottom dishes. After 1 hour, organoid media (DMEM-F12, 10% KnockOut Serum Replacement (Gibco), 1x Insulin-Transferrin-Selenium (Gibco), L-glutamine, penicillin/streptomycin) was added, and multiple phase-contrast and fluorescence images were taken at 0, 12, 24, 48, and 72 hours. Tube formation was quantified by tubes per high power field. Conditioned media for angiogenic secretome analysis was generated by culturing fibroblasts on BME in serum-free media for 24 hours prior to collection and analyzed using the Proteome Profiler Mouse Angiogenesis Array (R&D #ARY015).

In vivo model of stromal-specific calcineurin deletion

The University of Pennsylvania Animal Care and Use Committee approved all studies. Mice with inducible stromal-specific deletion of CNB were obtained by cross-breeding C57Bl/6 *CnB1*$^{fl/fl}$ mice (19) with C57Bl/6 Col1a1-Cre-ER(T) mice (JAX #016241) (20). Breeding cages were maintained using Cola1-Cre;*CnB*$^{fl/fl}$ crossed to *CnB*$^{fl/fl}$ to ensure hemizygosity of the Cre transgene. To acutely delete *CnB in vivo*, mice were given 1 mg tamoxifen in 100 μl peanut oil (Sigma-Aldrich) intraperitoneally daily for 5 days. Mice in tumor studies received 1–2 additional doses of tamoxifen per week to ensure *Cn* deletion in bone marrow-derived stromal cells. CN deletion was confirmed by Western blot for CNA in lung fibroblasts.

To confirm Col1a1-Cre-ER(T) mRNA expression in lung fibroblasts, cells were lysed in Trizol, RNA extracted with Zymo Direct-ZOL kits with on-column DNase digestion, followed by a cDNA Reverse Transcription Kit. 200ng of cDNAs per qPCR reaction were added to 2x SYBR Green qPCR Master Mix (Bimake). Primers: GAPDH: forward 5'-AGGTCGGTGTGAACGGATTTG-3' and reverse 5'-TGTAGACCATGTAGTTGAGGTCA-3', Col1a1-Cre: forward 5'-CCAGCCGCAAAGAGTCTACA-3' and reverse 5'-ACAATCAAGGGTCCCCAAAC-3'.

Injection-resection model of lung metastasis

Lewis lung carcinoma (LLC) cells were obtained from ATCC; MH6449 PDAC cells were a gift from Dr. Ben Stanger (University of Pennsylvania). Tumor cells were cultured in DMEM + 4 g/L glucose, 10% FBS, L-glutamine/pen-strep. Mice were 8–12 weeks old except where noted and 1×10^6 (PDAC) or 5×10^6 (LLC) tumor cells in 100 μl serum free DMEM were injected subcutaneously into the flank. Tumor volume was calculated with digital calipers and the ellipsoid volume equation $V = ½ * \text{width}^2 * \text{length}$. Tumors were resected at 400–600 mm^3 and flash-frozen in OCT with surgical sites closed using non-absorbable monofilament suture (Covidien). Mice received 5mg/kg Metacam for 3 days following resection and after 14 days, mice were euthanized, lungs perfused with saline, dissected and formalin-fixed for paraffin embedding or fixed in 4% PFA followed by incubation in 30% sucrose before freezing in OCT. FFPE samples were sectioned at 5 μM, and frozen samples were sectioned at 9–10 μM. Lung tumors were measured and normalized to total lung area using ImageJ software.

Cell line verification and testing

Primary cell identity were verified as described above. LLCs were obtained directly from ATCC and passaged for less than six months prior to use. MH6449 cells were originally generated by the Stanger lab and used or frozen within 6 months of receipt. *Mycoplasma* testing was not performed.

Statistical analysis

Statistical analysis was performed using GraphPad Prism 7. P values were calculated using Student's t-test (two-tailed, unpaired) or ANOVA where appropriate.

Results

CN deletion promotes fibroblast migration

Increased fibroblasts in benign and malignant diseases are attributed to fibroblast proliferation and migration, as well as recruitment of mesenchymal precursors from the bone marrow. Thus, we examined whether deletion of CN altered fibroblast proliferation. Primary lung fibroblasts derived from *CnB* floxed mice were treated with adenoviral Cre recombinase with deletion of *CnB* destabilizing the CNA subunit (19, Supplementary Figure S1). No differences were observed in cell proliferation between WT and $Cn^{-/-}$ fibroblasts (Figure 1A). However, in scratch assays of confluent monolayers, $Cn^{-/-}$ fibroblasts exhibited enhanced closure at 24 hours post-wounding (Figure 1B), and live-cell imaging over the first 24 hours post-scratch revealed that $Cn^{-/-}$ fibroblasts demonstrated accelerated and different migratory phenotypes compared to WT fibroblasts. $Cn^{-/-}$ fibroblasts migrated perpendicularly to the leading edge of the wound as compared to WT fibroblasts, which exhibited more stochastic motion throughout wound closure (Supplemental Video 1).

The accelerated closure by $Cn^{-/-}$ fibroblasts in scratch assays suggested that CN deletion increases fibroblast migration. Indeed, in uncoated transwell migration assays, $Cn^{-/-}$ fibroblasts exhibited greater migration compared to WT fibroblasts after 24 hours (Figure 1C). However, $Cn^{-/-}$ fibroblasts exhibited impaired migration compared to WT controls on transwells coated with type I collagen (Figure 1D), implicating CN-null fibroblasts are unable to invade and migrate through collagen. Collectively, these data indicate that while CN deletion increased fibroblast migration, it inhibited collagen invasion and had no effect on fibroblast proliferation.

CN-null fibroblasts exhibit increased collagen contractility and matrix remodeling

Another key function of activated fibroblasts is to process and remodel collagen, thus we plated fibroblasts onto thick type I collagen gels. Without fibroblasts, these collagen gels contain little fibrillar collagen as visualized by 2-photon second harmonic generation (SHG) imaging. Fibroblasts remodel and exert tension on the collagen substratum, forming a fibrillar network visible by SHG. $Cn^{-/-}$ fibroblasts remodeled type I collagen gels more than WT fibroblasts, leading to increased SHG signal (Figure 2A).

To further investigate the effects of CN deletion on collagen remodeling, we utilized a collagen contraction assay. Fibroblasts were embedded in type I collagen gels which were

detached triggering collagen remodeling and fibroblast exertion in the gel causing contraction (16). *Cn*$^{-/-}$ fibroblasts significantly increased the rate of collagen gel contraction at 6 and 12 hours post-detachment with maximal contraction by 12 hours. In contrast, WT fibroblasts required almost 20 hours post-detachment for maximal contraction (Figure 2B).

We assessed the ability of *Cn*$^{-/-}$ fibroblasts to deposit, accumulate and remodel collagen by comparing fibroblast-derived matrices (FDMs) from WT and *Cn*$^{-/-}$ fibroblasts (17). CN deletion led to significant increases in the accumulation of fibrillar collagen and alignment of collagen fibrils as observed by SHG imaging (Figure 2C). ECM is remodeled through multiple mechanisms, including the production of collagenases by fibroblasts, so we compared the collagenase activity associated with CN-null and WT fibroblasts by overlaying DQ™ type I collagen on fibroblasts cultured on collagen gels. DQ collagen is saturated with quenched fluorescein molecules, and digestion by collagenases releases fluorescent fragments of collagen. *Cn*$^{-/-}$ fibroblasts plated on either gelatin-coated chamber slides or a collagen substratum exhibited more collagenase activity than WT fibroblasts (Figure 2D-E). This was specific for collagenase activity, as we observed no difference in gelatinase activity under either culture condition. Collectively, our data indicate that CN deletion leads to increased collagen accumulation, remodeling, and contractility in the absence of activating stimuli, suggesting the importance of CN for fibroblast homeostasis.

Constitutively active NFAT signaling partially rescues CN deletion

To determine whether restoration of NFAT activation could rescue Cn$^{-/-}$ fibroblasts and limit fibroblast activation, we transduced *Cn*$^{-/-}$ fibroblasts with a constitutively nuclear NFATc1 mutant (caNFATc1) (Supplementary Figure S2), and assayed its effects on collagen remodeling and migration. Expression of caNFATc1 partially reversed the increased collagenase activity of *Cn*$^{-/-}$ fibroblasts in DQ type I collagen assays as compared to *Cn*$^{-/-}$ fibroblasts (Supplementary Figure S3). However, scratch assays on *Cn*$^{-/-}$ fibroblasts with caNFATc1 expression showed increased migration and a flattened morphology similar to *Cn*$^{-/-}$ fibroblasts (Supplementary Figure S4) and had a nominal effect on fibrillar collagen remodeling in fibroblasts cultured on type I collagen gels (Supplementary Figure S5). These data suggest that restoration of NFAT signaling decreases collagenase activity by CN-null fibroblasts, similar to WT fibroblasts, but does not significantly affect fibroblast migration or fibrillar collagen remodeling.

CN deletion alters collagen processing consistent with a CAF-like state

Given that higher fiber density and greater fiber alignment are characteristic of FDMs derived from cancer-associated fibroblasts, we compared WT and *Cn*$^{-/-}$ FDMs generated with normal media or tumor cell conditioned media (CM) from SR0144 cells, a murine lung adenocarcinoma cell line. As expected, when WT fibroblasts were cultured with tumor CM, we observed a greater accumulation of fibrillar collagen in the generated matrix as measured by SHG signal than in matrix generated in normal media. We also observed foci of more highly aligned collagen in FDMs generated by WT cells in the presence of tumor CM. Interestingly, we found that FDMs generated by *Cn*$^{-/-}$ fibroblasts in the presence of normal media exhibited similar increased accumulation of fibrillar collagen (Figure 3A). These data

suggest *Cn*$^{-/-}$ fibroblasts phenotypically resemble tumor cell CM-treated WT fibroblasts and do not respond to further stimulation by tumor CM.

We decellularized and examined *Cn*$^{-/-}$ and WT FDMs at earlier timepoints to examine matrix deposition and remodeling. After 3 days, there were noticeable differences in both fibroblast and matrix alignment in CN-null fibroblasts that were enhanced after 5 days (Figure 3B). Consistent with the increase in linear alignment of collagen fibrils in FDMs derived from *Cn*$^{-/-}$ fibroblasts, the cells themselves were more linearly aligned and elongated.

Altered matrix remodeling by Cn-null fibroblasts causes cytoskeletal reorganization in fibroblasts and tumor cells

Our data show that CN regulates fibroblast-mediated matrix remodeling. It is well-established that alterations in matrix organization drive cytoskeletal reorganization, cell size and shape. Thus, we compared how FDMs derived from WT and CN-null fibroblasts affected the actin cytoskeleton in fibroblasts and tumor cells. When WT fibroblasts were plated on *Cn*$^{-/-}$ FDMs and stained for phalloidin and the focal adhesion complex protein paxillin, they displayed long, thin cytoplasmic processes and an elongated morphology compared to their behavior on WT FDMs (Figure 4A). Similar to WT fibroblasts, PDACs cultured on FDMs derived from *Cn*$^{-/-}$ fibroblasts were also elongated (Figure 4B), and live-cell imaging of PDACs on these FDMs revealed greater displacement and more linear movement on *Cn*$^{-/-}$ FDMs as compared to WT FDMs (Figure 4C-D, Supplemental Video 2). Lewis lung carcinoma (LLC) tumor cells were similarly elongated on *Cn*$^{-/-}$ FDMs (Supplemental Figure S6), but unlike PDACs, there was no difference in their migratory behavior. Therefore, the matrix generated by *Cn*$^{-/-}$ fibroblasts is sufficient to significantly alter the cytoskeletal architecture of both tumor cells and fibroblasts compared to WT fibroblasts.

Loss of CN in fibroblasts promotes EC tube formation

Activated fibroblasts and their associated matrix play a crucial role in angiogenesis both by providing structural support and by secreting pro-angiogenic factors. We co-cultured primary lung ECs with WT or *Cn*$^{-/-}$ fibroblasts on BME, and found that *Cn*$^{-/-}$ as compared to WT fibroblasts, supported more robust EC tube formation measured by \tube segments and branch points (Figure 5A).

To examine if the impact on EC tube formation was due to changes in production of angiogenic factors, we compared the secretome of WT and *Cn*$^{-/-}$ fibroblasts. Conditioned media from WT and *Cn*$^{-/-}$ fibroblasts cultured on BME were probed for angiogenesis-related proteins and showed significant upregulation of multiple cytokines and growth factors by CN-null as compared to WT fibroblasts. Notably, SDF-1, a chemokine that promotes angiogenesis as well as a myofibroblast phenotype in both cancer and fibrotic disease, was increased in *Cn*$^{-/-}$ fibroblast CM (Figure 5B) (21-24). Thus, the differences observed in our *in vitro* tube formation assays may be partially mediated by differences in angiogenic secreted factors.

Loss of CN in fibroblasts promotes tumor progression

Our data suggest that CN deletion in fibroblasts leads to an activated phenotype in fibroblasts that is pro-tumorigenic. To investigate tumor growth and metastases in mice with fibroblast specific deletion of CN, we cross-bred $Cn^{fl/fl}$ mice with transgenic mice expressing tamoxifen-inducible Cre driven by a type I collagen alpha-1 chain promoter (Col1a1-Cre-ER(T)) (20,25) to delete CN from the stroma. We confirmed Cre expression in lung fibroblasts as well as a significant decrease in CN expression in these cells 1 week after tamoxifen administration (Figure 6A-B).

To examine both primary tumor growth and metastases, we utilized an injection-resection model of spontaneous lung metastasis using LLC and MH6449 PDAC tumor cell lines. Following tamoxifen injection in syngeneic *Col1a1-Cre;*$Cn^{fl/fl}$ mice, subcutaneous tumors were established and resected at 400–600 mm^3. Fourteen days following resection, mice were were analyzed for lung metastases (Figure 6C). There was no difference in primary tumor growth between $Cn^{fl/fl}$ (WT) and *Col1a1-Cre;*$Cn^{\Delta/\Delta}$ mice (Figure 6D), however, there was an increase in the size of LLC lung metastases and a trend towards larger PDAC lung metastases in *Col1a1-Cre;*$Cn^{\Delta/\Delta}$ mice (Figure 6E). Additionally, 6/6 of stromal $Cn^{\Delta/\Delta}$ vs 4/6 WT mice in the LLC and 4/6 vs 2/6 in the PDAC model developed visible lung metastases, indicating an increase in the development of lung metastases upon CN deletion in lung fibroblasts (Figure 6F). These data suggest that stromal deletion of CN specifically increases both the colonization and outgrowth of lung metastases.

Discussion

Here we show that CN deletion in fibroblasts leads to functional alterations consistent with an activated, pro-tumorigenic fibroblast phenotype. We demonstrate that $Cn^{-/-}$ fibroblasts exhibited greater migratory capacity during scratch assays and transwell migration assays; however, they do not invade type I collagen gels to the same extent as WT. Our studies identified a role for CN in the deposition and remodeling of ECM, particularly collagen, with $Cn^{-/-}$ fibroblasts exhibiting increased collagenase activity and collagen remodeling. CN deletion led to an increase in fibrillar collagen in $Cn^{-/-}$ fibroblast-derived matrices and when cultured on type I collagen gels. These differences in matrix alter the cytoskeletal reorganization of both fibroblasts and tumor cells, with tumor cells exhibiting more linearly directed movement when cultured on $Cn^{-/-}$ matrix. Our *in vitro* studies show that CN-null fibroblasts increase their production of angiogenesis-related proteins and promote EC tube formation while fibroblast-specific deletion of CN in mice show increased incidence and size of lung metastases in an experimental model of metastasis. Our data suggest that CN deletion leads to an activated fibroblast phenotype without stimuli, phenocopying cancer-associated, pro-tumorigenic fibroblasts. This suggests CN may play a crucial role in the maintenance of fibroblast homeostasis or the “un-activated” state.

We show that CN deletion increases the migration of fibroblasts, but decreases their invasion through type I collagen. Given that $Cn^{-/-}$ fibroblasts demonstrated increased collagenase activity in other assays, it is unlikely that this is caused by a decrease in collagen proteolysis. It is possible that the increase in fibrillar collagen of $Cn^{-/-}$ fibroblasts on type I collagen gels engage integrins with specificity for collagen triple helical fibrils, such as integrins $\alpha 1\beta 1$

and α2β1 (26). This remodeling phenotype may promote interactivity with the collagen substratum instead of invasion through it.

Our work also identifies a role for CN in the secretion and remodeling of ECM, specifically collagen. *Cn*$^{-/-}$ fibroblasts remodel and exert contractile forces on collagen substrates as well as secrete and remodel new ECM to a greater extent than WT fibroblasts. However, we observed no difference in gelatinase activity, suggesting that CN specifically regulates the processing of fibrillar collagen and not its denatured form, possibly through differential expression of collagenases. Matrices derived from *Cn*$^{-/-}$ fibroblasts have greater and more linearly aligned fibrillar collagen consistent with FDMs generated from cancer-associated fibroblasts (27). In support of this, WT FDMs generated in the presence of tumor-conditioned media resemble *Cn*$^{-/-}$ FDMs generated in normal growth media.

We demonstrated that *Cn*$^{-/-}$ fibroblast-derived matrix directs the cytoskeletal architecture of both WT fibroblasts and PDAC tumor cells, causing an increased aspect ratio. The elongation of PDACs on *Cn*$^{-/-}$ FDMs may indicate increased epithelial-to-mesenchymal transition compared to PDACs cultured on WT FDMs. The straightness of tumor cell migration paths and right-skewing of the mean square displacement distribution on *Cn*$^{-/-}$ FDMs corresponds to increased migration along more linearly aligned collagen fibrils, also frequently observed in tumor invasion (28).

We propose that the alterations in collagen fiber architecture observed may inform the increased incidence and size of metastases in stromal CN-null mice in our experimental metastasis model. We did not observe gross differences in collagen fiber morphology or density, or in microvessel density in PDAC primary tumors; however, at the time of resection, these tumors were well past the angiogenic and stromagenic switch (2,29). Differences in ECM architecture and angiogenesis at earlier time points may be masked by analysis of large tumors after resection, despite no difference in primary tumor growth.

Our work identifies CN as a key pathway regulating fibroblast homeostasis as CN deletion leads to activation in the absence of activating stimuli. While our work identifies a role for CN in fibroblast homeostasis, CN deletion has been shown to disrupt homeostasis in other cells and disease models (30-33). The role of CN/NFAT signaling in fibroblast activation is complex. Evidence exists for both pro- and anti-fibrotic effects of CN/NFAT signaling in fibroblasts isolated from a variety of tissues (34-42). It is important to note that some studies used pharmacologic inhibition of CN via cyclosporin A (CsA); we and others have shown that CsA has a significant number of CN-independent targets and effects (43,44), and the anti-fibrotic effects of CsA in one study were not recapitulated with tacrolimus, a CN inhibitor with a different mechanism of action (45). Therefore, it is possible that CsA-mediated anti-fibrotic phenotypes are off-target effects.

It is unclear whether the activated phenotype of *Cn*$^{-/-}$ fibroblasts is dependent on NFAT signaling, as CN has targets besides NFAT (13,46). Studies suggest that NFAT is activated in response to stimuli such as mechanical stretching or TGF-β treatment (39,47); however, constitutively active NFAT has been shown to suppress myofibroblast transdifferentiation (48). An NFAT target that may promote EC tube formation and increase metastases is

SDF-1/CXCL12, a pro-fibrotic and pro-angiogenic chemokine that was upregulated in $Cn^{-/-}$ fibroblast secretome when cultured on type I collagen gels and fibronectin-coated hydrogels. Some evidence exists for the negative regulation of SDF-1 by NFAT in osteoblasts (49) and cytotrophoblast cells (50). Thus, one mechanism by which CN deletion leads to a pro-tumorigenic phenotype in fibroblasts may be via SDF-1 expression. However, we also demonstrated that constitutively active NFAT signaling only partially rescues CN-null fibroblast phenotypes, suggesting NFAT-independent effects as well.

Of note, our work specifically studied the role of CN in lung fibroblasts. It is known that fibroblasts display organ specific gene expression patterns and different cancers display differential levels of fibroblast activation. However, the function of activated stromal cells is similar across different organ and diseases (51,52); thus, it is likely that CN modulates fibroblast activation in other organ stroma as well.

Collectively, our data demonstrate a role for CN signaling in fibroblast homeostasis with CN deletion promoting a pro-tumorigenic, activated phenotype in primary lung fibroblasts, and that stromal deletion of CN *in vivo* leads to an increase in the incidence and size of lung metastases. One important implication of our work is an alternative mechanism by which chronic CN inhibition in transplant patients leads to increased malignancy. Previously, CN inhibitor-induced malignancy had been assumed to occur due to immunosuppression (53) however, our data implicate stromal effects as another mechanism by which CsA increases tumorigenesis. Translational potential of this work includes targeting CN signaling to abrogate stromal cell activation during metastatic progression. Elucidation of NFAT-dependent and independent targets in lung fibroblasts may identify specific signaling pathways that maintain fibroblast homeostasis and are amenable to pharmacologic targeting.

Supplementary Material

Refer to Web version on PubMed Central for supplementary material.

Acknowledgements

We acknowledge Dr. Carla Kim and Dr. Ben Stanger for generously providing tumor cell lines. We thank Priya Govindaraju, Rachel Blomberg and Kerry Roby for their technical assistance. We acknowledge our funding sources: NCI F30 CA 196079 (A. Lieberman), NCI R01 CA172921 (E. Puré), and NCI R01 CA 118374 (S. Ryeom).

References

1. Balkwill FR, Capasso M, Hagemann T. The tumor microenvironment at a glance. J Cell Sci. 2012;125:5591–6. [PubMed: 23420197]
2. Pure E, Lo A. Can Targeting Stroma Pave the Way to Enhanced Antitumor Immunity and Immunotherapy of Solid Tumors? Cancer Immunol Res. 2016;4:269–78. [PubMed: 27036971]
3. Olumi AF, Grossfeld GD, Hayward SW, Carroll PR, Tlsty TD, Cunha GR. Carcinoma-associated Fibroblasts Direct Tumor Progression of Initiated Human Prostatic Epithelium. Cancer Res. 1999;59:5002–11. [PubMed: 10519415]
4. Jacob M, Chang L, Puré E. Fibroblast activation protein in remodeling tissues. Curr Mol Med. 2012;12:1220–43. [PubMed: 22834826]
5. Puré E, Blomberg R. Pro-tumorigenic roles of fibroblast activation protein in cancer: back to the basics Oncogene. Springer US; 2018;37:4343–57. [PubMed: 29720723]

6. Hinz B, Celetta G, Tomasek JJ, Gabbiani G, Chaponnier C. Alpha-Smooth Muscle Actin Expression Upregulates Fibroblast Contractile Activity. Mol Biol Cell. 2001;12:2730–41. [PubMed: 11553712]
7. Chang HY, Chi J-T, Dudoit S, Bondre C, van de Rijn M, Botstein D, et al. Diversity, topographic differentiation, and positional memory in human fibroblasts. Proc Natl Acad Sci. 2002;99:12877–82. [PubMed: 12297622]
8. Kalluri R, Zeisberg M. Fibroblasts in cancer. Nat Rev Cancer. 2006;6:392–401. [PubMed: 16572188]
9. Kotas ME, Medzhitov R. Homeostasis, Inflammation, and Disease Susceptibility Cell. Elsevier Inc.; 2015;160:816–27. [PubMed: 25723161]
10. Minami T, Jiang S, Schadler K, Suehiro J-I, Osawa T, Oike Y, et al. The calcineurin-NFAT-angiopoietin-2 signaling axis in lung endothelium is critical for the establishment of lung metastases. Cell Rep. The Authors; 2013;4:709–23. [PubMed: 23954784]
11. Ryeom S, Baek K-H, Rioth MJ, Lynch RC, Zaslavsky A, Birsner A, et al. Targeted deletion of the calcineurin inhibitor DSCR1 suppresses tumor growth. Cancer Cell. 2008;13:420–31. [PubMed: 18455125]
12. Baek K-H, Zaslavsky A, Lynch RC, Britt C, Okada Y, Siarey RJ, et al. Down Syndrome Suppression of Tumor Growth and the Role of the Calcineurin Inhibitor DSCR1. Nature. 2009;459:1126–30. [PubMed: 19458618]
13. Rusnak F, Mertz P. Calcineurin: form and function. Physiol Rev. 2000;80:1483–521. [PubMed: 11015619]
14. Mancini M, Toker A. NFAT proteins: emerging roles in cancer progression Nat Rev Cancer. Nature Publishing Group; 2009;9:810–20. [PubMed: 19851316]
15. Acharya PS, Majumdar S, Jacob M, Hayden J, Mrass P, Weninger W, et al. Fibroblast migration is mediated by CD44-dependent TGF β activation. 2008.
16. Grinnell F, Ho CH, Lin YC, Skuta G. Differences in the regulation of fibroblast contraction of floating versus stressed collagen matrices. J Biol Chem. 1999;274:918–23. [PubMed: 9873032]
17. Castelló-cros R, Cukierman E. Extracellular Matrix Protocols. Even-Ram S, Artym V, editors. Totowa, NJ: Humana Press; 2009.
18. Lee J-H, Bhang DH, Beede A, Huang TL, Stripp BR, Bloch KD, et al. Lung stem cell differentiation in mice directed by endothelial cells via a BMP4-NFATc1-thrombospondin-1 axis Cell. Elsevier; 2014;156:440–55. [PubMed: 24485453]
19. Neilson JR, Winslow MM, Hur EM, Crabtree GR. Calcineurin B1 is essential for positive but not negative selection during thymocyte development. Immunity. 2004;20:255–66. [PubMed: 15030770]
20. Kim J-E, Nakashima K, de Crombrugghe B. Transgenic Mice Expressing a Ligand-Inducible Cre Recombinase in Osteoblasts and Odontoblasts. Am J Pathol. 2004;165:1875–82. [PubMed: 15579432]
21. Orimo A, Gupta PB, Sgroi DC, Arenzana-Seisdedos F, Delaunay T, Naeem R, et al. Stromal fibroblasts present in invasive human breast carcinomas promote tumor growth and angiogenesis through elevated SDF-1/CXCL12 secretion. Cell. 2005;121:335–48. [PubMed: 15882617]
22. Kojima Y, Acar A, Eaton EN, Mellody KT, Scheel C, Ben-Porath I, et al. Autocrine TGF-beta and stromal cell-derived factor-1 (SDF-1) signaling drives the evolution of tumor-promoting mammary stromal myofibroblasts. Proc Natl Acad Sci U S A. 2010;107:20009–14. [PubMed: 21041659]
23. Xu J, Mora A, Shim H, Stecenko A, Brigham KL, Rojas M. Role of the SDF-1 / CXCR4 Axis in the Pathogenesis of Lung Injury and Fibrosis. 2007.
24. Jackson EK, Zhang Y, Gillespie DD, Zhu X, Cheng D, Jackson TC. SDF-1α (stromal cell-derived factor 1α) induces cardiac fibroblasts, renal microvascular smooth muscle cells, and glomerular mesangial cells to proliferate, cause hypertrophy, and produce collagen. J Am Heart Assoc. 2017;6:1–20.
25. Rossert J, Eberspaecher H, De Crombrugghe B. Separate cis-acting DNA elements of the mouse pro-alpha1(I) collagen promoter direct expression of reporter genes to different type I collagen-producing cells in transgenic mice. 1995;129:1421–32.
26. Barczyk M, Carracedo S, Gullberg D. Integrins. Cell Tissue Res. 2010;339:269–80. [PubMed: 19693543]

27. Malik R, Lelkes PI, Cukierman E. Biomechanical and biochemical remodeling of stromal extracellular matrix in cancer. Trends Biotechnol. 2015;33:230–6. [PubMed: 25708906]
28. Han W, Chen S, Yuan W, Fan Q, Tian J, Wang X, et al. Oriented collagen fibers direct tumor cell intravasation. Proc Natl Acad Sci. 2016;113:11208–13. [PubMed: 27663743]
29. Bergers G, Benjamin LE. Tumorigenesis and the angiogenic switch. Nat Rev Cancer. 2003;3:401–10. [PubMed: 12778130]
30. Wang X, Bi Y, Xue L, Liao J, Chen X, Lu Y, et al. Calcineurin-NFAT axis controls allograft immunity in myeloid-derived suppressor cells through reprogramming T cell differentiation. Mol Cell Biol. 2014;35:598–609. [PubMed: 25452304]
31. Fric J, Zelante T, Wong AYW, Mertes A, Yu HB, Ricciardi-Castagnoli P. NFAT control of innate immunity. Blood. 2012;120:1380–9. [PubMed: 22611159]
32. Dotto GP. Calcineurin Signaling as a Negative Determinant of Keratinocyte Cancer Stem Cell Potential and Carcinogenesis. Cancer Res. 2011;71:2029–33. [PubMed: 21406393]
33. Arendt KL, Zhang Z, Ganesan S, Hintze M, Shin MM, Tang Y, et al. Calcineurin mediates homeostatic synaptic plasticity by regulating retinoic acid synthesis. Proc Natl Acad Sci. 2015;112:E5744–52. [PubMed: 26443861]
34. Fellström B Cyclosporine nephrotoxicity. Transplant Proc. 2004;36:S220–3.
35. Rush D The impact of calcineurin inhibitors on graft survival Transplant. Rev. Elsevier Inc; 2013 page 93–5.
36. Moreno J, Cuervas-Mons V, Rubio E, Pons F, Herreros de TA, Turrión V, et al. Chronic renal dysfunction after liver transplantation in adult patients: prevalence, risk factors, and impact on mortality. Transplant Proc. 2003;35:1907–8. [PubMed: 12962843]
37. Johnson DW, Saunders HJ, Johnson FJ, Huq SO, Field MJ, Pollock CA. Cyclosporin exerts a direct fibrogenic effect on human tubulointerstitial cells: roles of insulin-like growth factor I, transforming growth factor beta1, and platelet-derived growth factor. J Pharmacol Exp Ther. 1999;289:535–42. [PubMed: 10087047]
38. Gooch JL, Roberts BR, Cobbs SL, Tumlin JA. Loss of the α-isoform of calcineurin is sufficient to induce nephrotoxicity and altered expression of transforming growth factor-β. Transplantation. 2007;83:439–47. [PubMed: 17318077]
39. Herum KM, Lunde IG, Skrbic B, Florholmen G, Behmen D, Sjaastad I, et al. Syndecan-4 signaling via NFAT regulates extracellular matrix production and cardiac myofibroblast differentiation in response to mechanical stress J Mol Cell Cardiol. Elsevier Ltd; 2013;54:73–81. [PubMed: 23178899]
40. Wilkins BJ, Molkentin JD. Calcium-calcineurin signaling in the regulation of cardiac hypertrophy. Biochem Biophys Res Commun. 2004;322:1178–91. [PubMed: 15336966]
41. Davis J, Burr AR, Davis GF, Birnbaumer L, Molkentin JD. A TRPC6-Dependent Pathway for Myofibroblast Transdifferentiation and Wound Healing In Vivo Dev Cell. Elsevier Inc.; 2012;23:705–15. [PubMed: 23022034]
42. Hirota N, Ito T, Miyazaki S, Ebina M, Homma S. Gene Expression Profiling of Lung Myofibroblasts Reveals the Anti-Fibrotic Effects of Cyclosporine. 2014;283–93.
43. Zhou AY, Ryeom S. Cyclosporin a promotes tumor angiogenesis in a calcineurin-independent manner by increasing mitochondrial reactive oxygen species. Mol Cancer Res. 2014;12:1663–76. [PubMed: 25009293]
44. Hu G, Wang K, Groenendyk J, Barakat K, Mizianty MJ, Ruan J, et al. Human structural proteome-wide characterization of Cyclosporine a targets. Bioinformatics. 2014;30:3561–6. [PubMed: 25172926]
45. Yamazaki R, Kasuya Y, Fujita T, Umezawa H, Yanagihara M, Nakamura H, et al. Antifibrotic effects of cyclosporine A on TGF- b 1 – treated lung fibroblasts and lungs from bleomycin-treated mice: role of hypoxia-inducible factor-1 a. 2018.
46. Li H, Rao A, Hogan PG. Interaction of calcineurin with substrates and targeting proteins. Trends Cell Biol. 2011;21:91–103. [PubMed: 21115349]
47. Gooch JL, Gorin Y, Zhang B-X, Abboud HE. Involvement of calcineurin in transforming growth factor-beta-mediated regulation of extracellular matrix accumulation. J Biol Chem. 2004;279:15561–70. [PubMed: 14742441]

48. Nishida M, Onohara N, Sato Y, Suda R, Ogushi M, Tanabe S, et al. Gα12/13-mediated up-regulation of TRPC6 negatively regulates endothelin-1-induced cardiac myofibroblast formation and collagen synthesis through nuclear factor of activated T cells activation. J Biol Chem. 2007;282:23117–28. [PubMed: 17533154]

49. Sesler CL, Zayzafoon M. NFAT signaling in osteoblasts regulates the hematopoietic niche in the bone microenvironment. Clin Dev Immunol. 2013;2013.

50. Du MR, Zhou WH, Piao HL, Li MQ, Tang CL, Li DJ. Cyclosporin A promotes crosstalk between human cytotrophoblast and decidual stromal cell through up-regulating CXCL12/CXCR4 interaction. Hum Reprod. 2012;27:1955–65. [PubMed: 22495096]

51. Kalluri R The biology and function of fibroblasts in cancer Nat Rev Cancer. Nature Publishing Group; 2016;16:582–98. [PubMed: 27550820]

52. Flier J, Underhill L, Dvorak H. Tumors: wounds that do not heal. N Engl J Med 1986;315:1650–9. [PubMed: 3537791]

53. Durnian JM, Stewart RMK, Tatham R, Batterbury M, Kaye SB. Cyclosporin-A associated malignancy. Clin Ophthalmol. 2007;1:421–30. [PubMed: 19668519]

Significance

Calcineurin signaling is a key pathway underlying fibroblast homeostasis that could be targeted to potentially prevent fibroblast activation in distant metastatic sites.

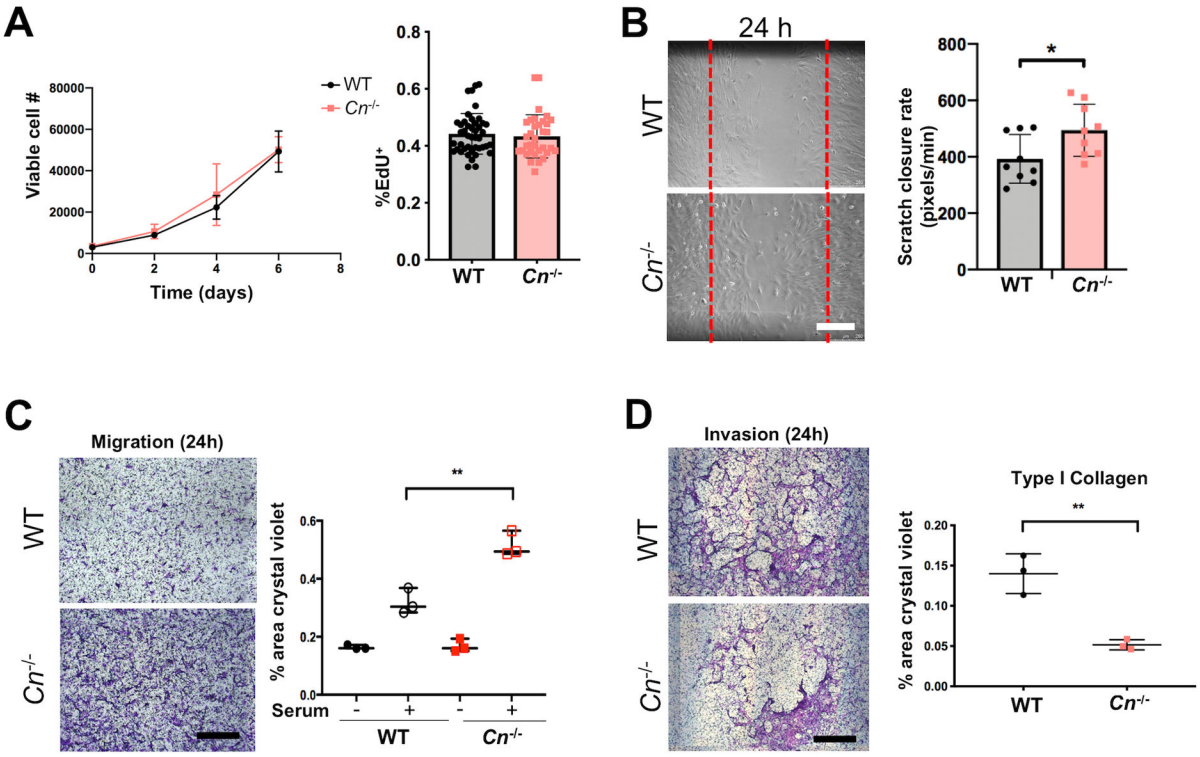

Figure 1: Calcineurin deletion promotes fibroblast migration but inhibits invasion.

A. WT and *Cn*$^{-/-}$ lung fibroblasts were counted on the indicated days after plating in normal growth media, and proliferation was assayed by EdU uptake (24 hour pulse). Cell counts are pooled from 2 separate experiments. **B.** Representative images from scratch assay at indicated time after scratch. Red dotted lines: width of scratch at 0 hour time point. Scratch closure rate was calculated using the change in scratch area over time for 18 images (N=9 each WT and *Cn*$^{-/-}$). Magnification bar = 250 μm. N=4 experimental replicates. **C.** Representative images and quantification of transwell migration assays. WT or *Cn*$^{-/-}$ fibroblasts were plated in serum-free media in the upper chamber of transwells and migrated toward serum-containing media in lower chamber. Migration was assessed after 24 hours by staining with crystal violet. **D.** Fibroblast invasion assays on transwells coated with type I rat tail collagen demonstrate decreased migration toward serum-containing media by *Cn*$^{-/-}$ fibroblasts after 18 hours. C,D bar = 500 μm. All samples were performed in triplicate; N=3 for migration, N=2 for collagen invasion. *p<0.05, **p<0.01. Error bars = standard deviation.

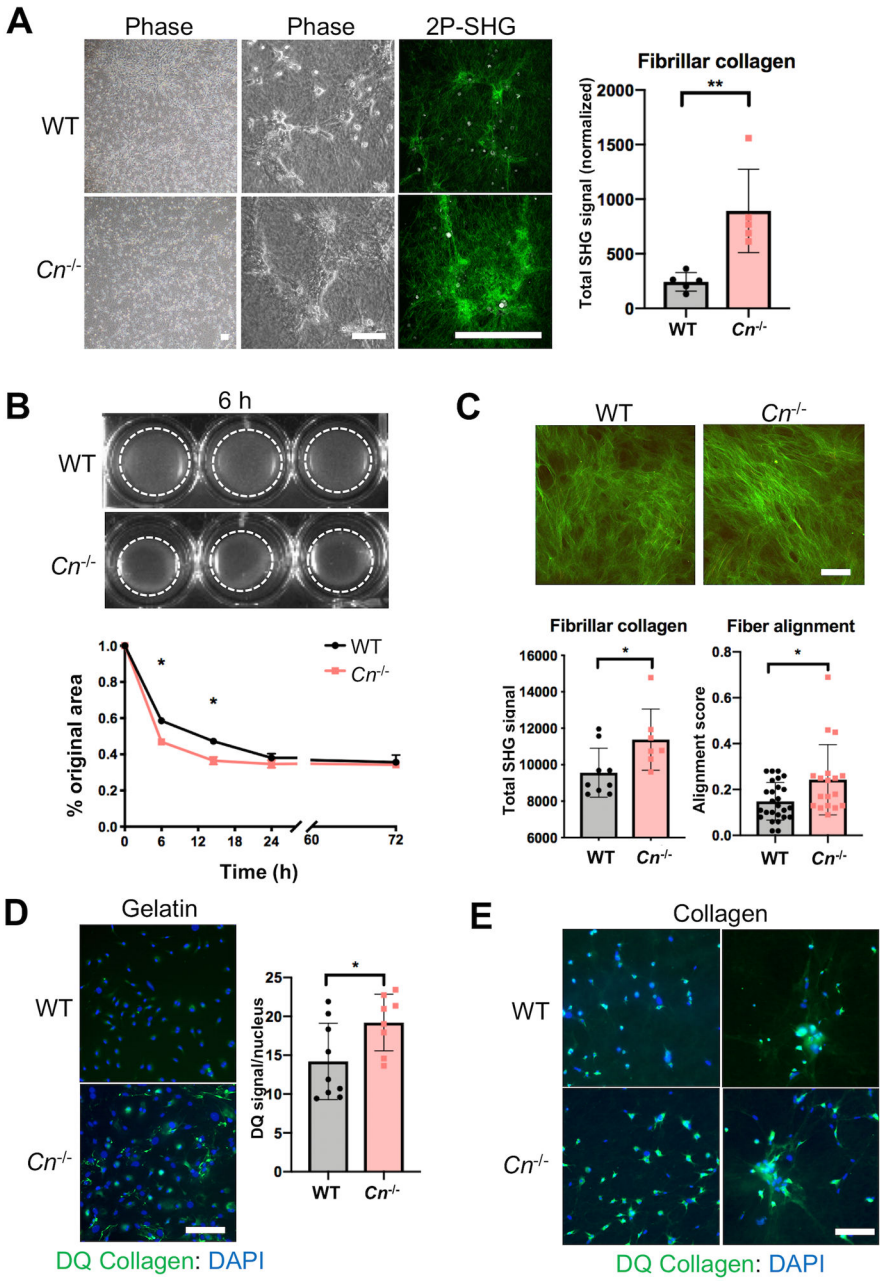

Figure 2: Calcineurin-null fibroblasts exhibit increased collagen contractility and matrix remodeling.

A. Phase-contrast and 2-photon second harmonic generation (2P-SHG) images of WT and *Cn*$^{-/-}$ fibroblasts cultured on collagen gels in serum-containing media for 48 hours. Total SHG signal (green) was quantified using ImageJ and normalized to cell count as measured by autofluorescent signal (white). N=5 fields from 2 technical replicates. Magnification bar = 250 μm. **B.** Representative images (after 6 hours) and quantification of collagen contraction by WT and *Cn*$^{-/-}$ fibroblasts at indicated times. White dotted lines denote collagen gel circumference. **C.** Representative 2P-SHG images of fibroblast-derived matrices. Total SHG signal (green) was quantified using ImageJ, and collagen fiber

alignment scores were determined using CurveAlign software. Bar = 100 μm. Data from 1 representative experiment for SHG signal and pooled from all replicates for alignment score, N=4 experimental replicates with 2-4 images per FDM. **D.** Images from DQ collagen assay on gelatin-coated glass and quantification of average DQ signal per nucleus using ImageJ. **E.** Images from DQ collagen assay on type I collagen gels. Collagenase-digested DQ™ collagen signal is green and nuclei (DAPI stain) are blue. Bar = 250 μm. DQ images from 1 representative experiment, N=3 experimental replicates. All samples were assayed in triplicate. *$p<0.05$, **$p<0.01$. Error bars = standard deviation.

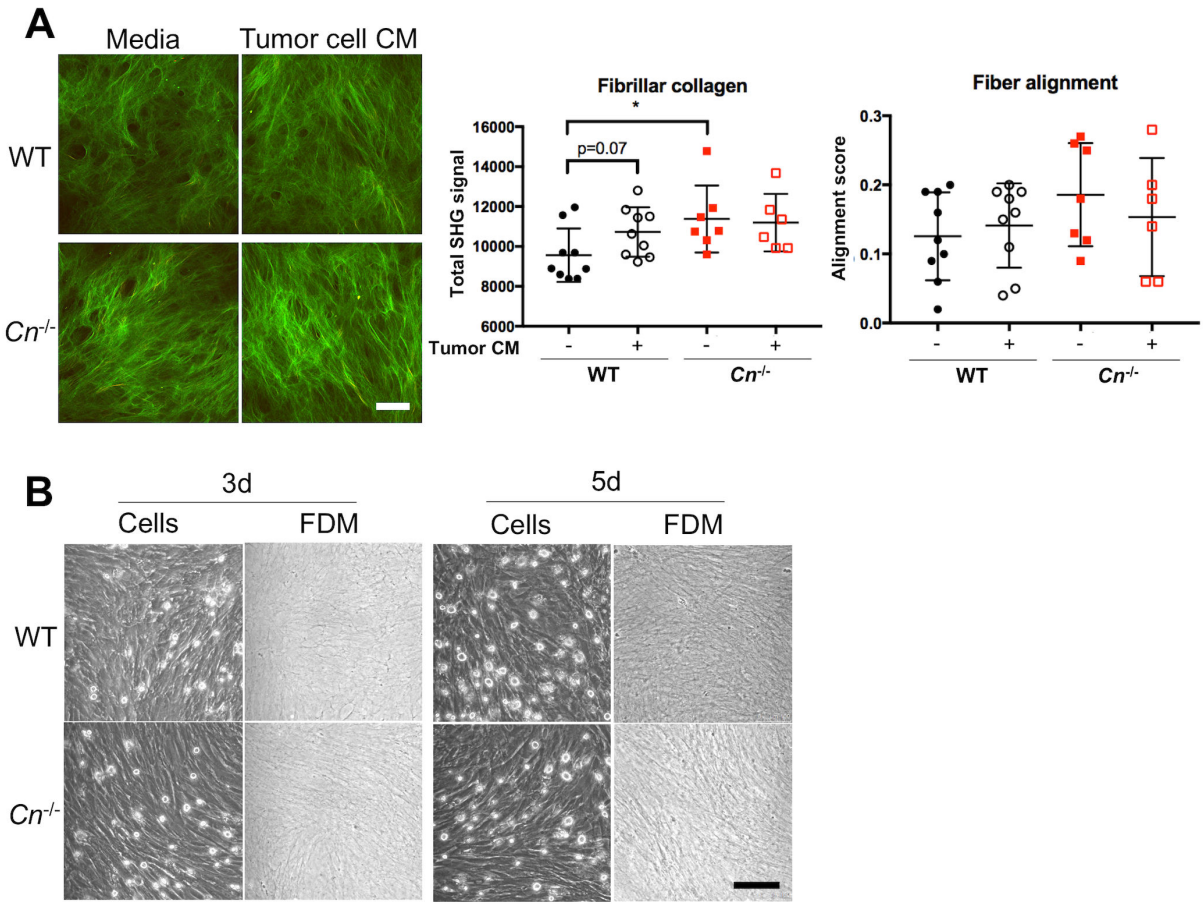

Figure 3: Calcineurin deletion leads to alterations in collagen processing consistent with a CAF-like state.

A. SHG images of WT or *Cn*$^{-/}$ fibroblast-derived matrices (FDMs) with and without lung tumor conditioned media. Total SHG signal (in green) was measured using ImageJ, and collagen fiber alignment scores were determined using CurveAlign software. Bar=100 μm. N=2 (3-5 fields per FDM imaged). **B.** Phase-contrast images of WT and *Cn*$^{-/-}$ fibroblasts and fibroblast-derived matrices (FDMs) following 3 and 5 days of ascorbate treatment. Bar = 100 μm. N=3 (3–5 fields per FDM imaged), *p<0.05. Error bar = standard deviation.

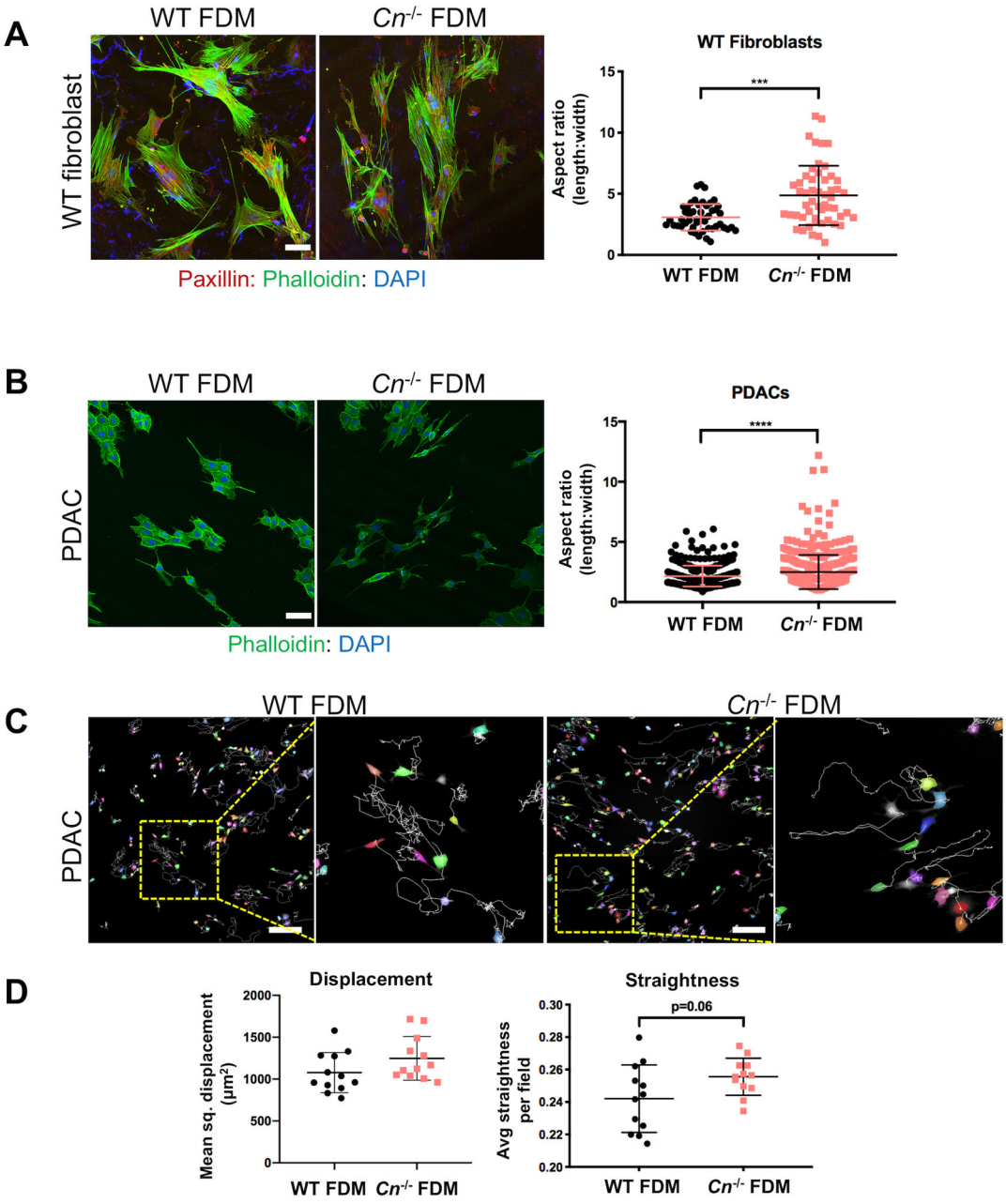

Figure 4: Calcineurin-null fibroblast-derived matrices induce cytoskeletal reorganization.

A. Confocal images of WT fibroblasts cultured on WT or $Cn^{-/-}$ fibroblast-derived matrix (FDM) and stained with paxillin (red), phalloidin (green), and DAPI (blue). Aspect ratio was calculated by dividing the width by the length for each cell. Bar = 50 μm. **B.** Confocal images of MH6449 PDAC cells cultured on WT or $Cn^{-/-}$ FDMs and stained with phalloidin (green) and DAPI (blue). Bar = 50 μm. Assay was performed in triplicate. ***p<0.001, ****p<0.0001. **C.** Representative live-cell tracking images of PDACs on WT or $Cn^{-/-}$ FDMs with magnified representative area denoted by dotted yellow box. Each line is an individual cell's path over 24 hours. Bar = 200 μm. **D.** Quantification of mean square displacement and straightness of cell track. Each data point represents the average value

from all cell tracks in 1 image. Assay was performed in duplicate, values pooled from N=6 images/videos per replicate. Error bar = standard deviation.

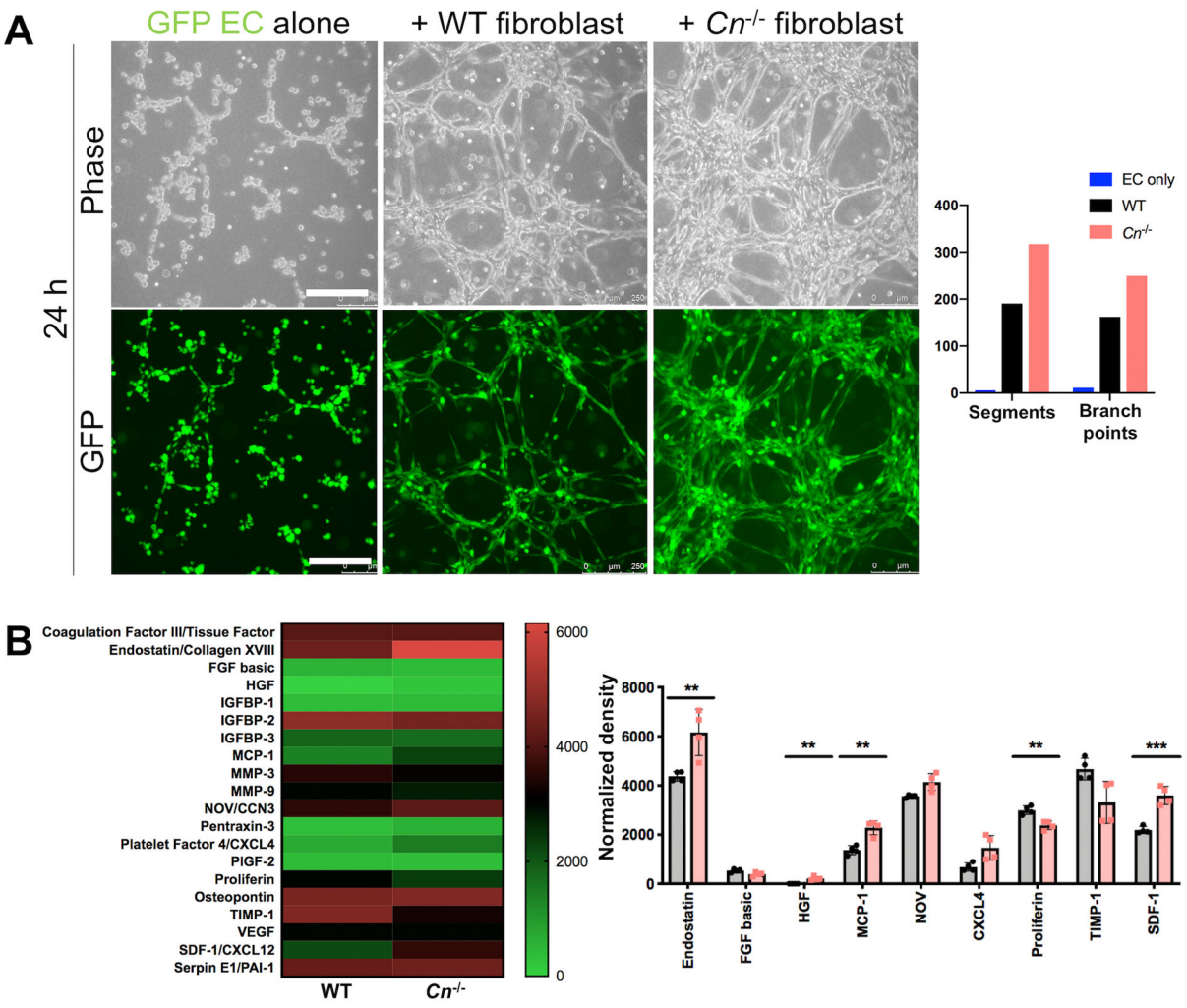

Figure 5: $Cn^{-/-}$ fibroblasts promote endothelial cell tube formation.

A. Representative images from tube formation assay with WT vs $Cn^{-/-}$ fibroblast + GFP^{+} endothelial cell (EC, green) co-cultures embedded in basement membrane extract (BME) at 24h following plating. Images are from 1 representative experiment (N=2 images from 1 replicate for quantification) of 6 experimental replicates. Quantification was performed on phase images using the Angiogenesis Analyzer tool in ImageJ. **B.** Conditioned media from WT or $Cn^{-/-}$ fibroblasts cultured on BME for 24 hours was analyzed with an angiogenesis antibody array. Cytokines with statistically significant differences between WT and $Cn^{-/-}$ fibroblasts ($p<0.05$) are quantified on right. **$p<0.01$, ***$p<0.001$. N=2 per condition; array contained technical duplicates for each cytokine. Error bar = standard deviation.

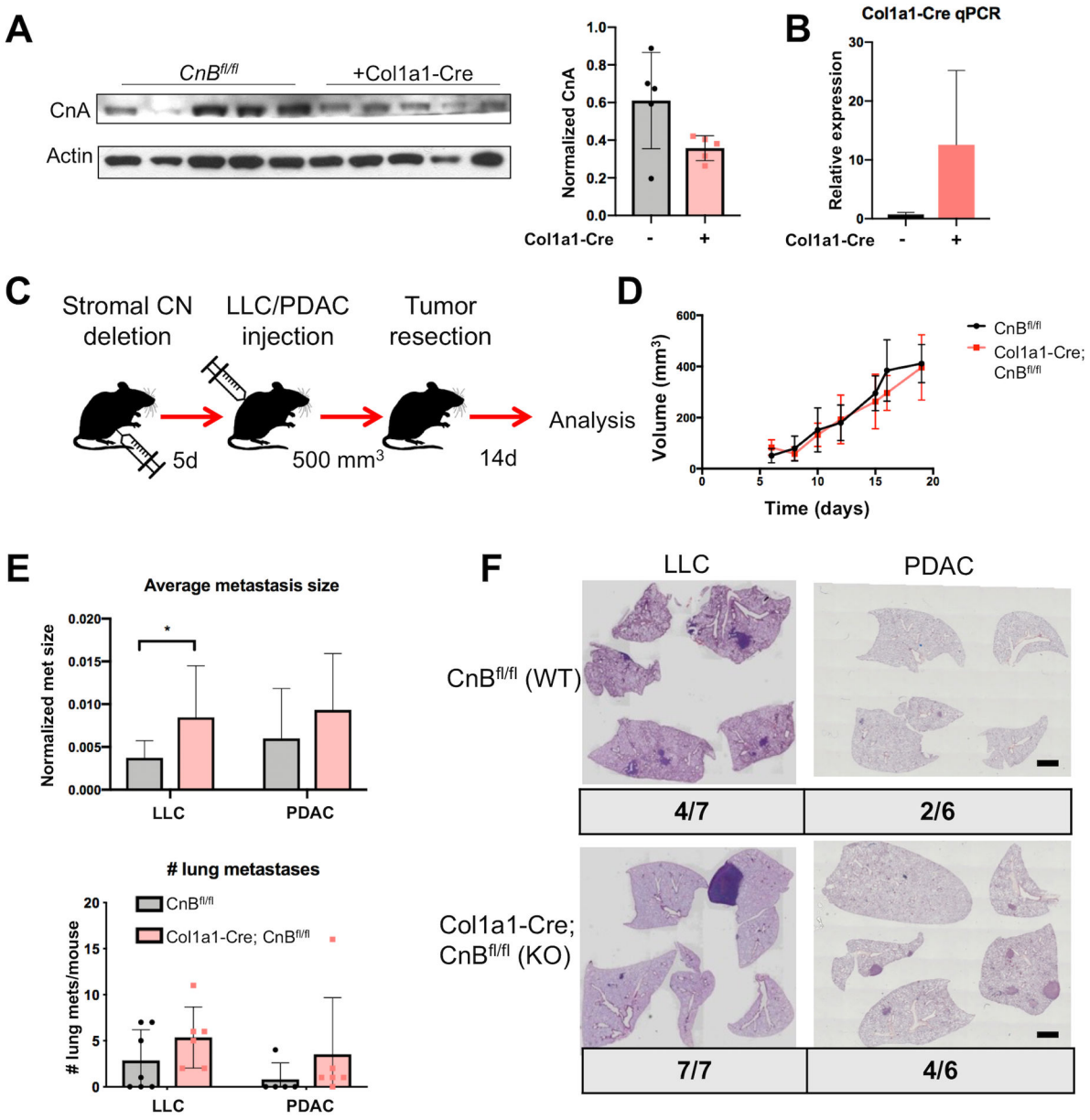

Figure 6: Stromal deletion of calcineurin increases the incidence and size of lung metastases.

A. Confirmation of stromal *Cn* knockdown in lung fibroblasts from Col1a1-Cre-ER(T);*CnB*$^{fl/fl}$ mice by Western blot for CnA. **B.** qPCR for Col1a1-Cre. Each lane represents lung fibroblasts isolated from 1 mouse. **C.** Schematic of injection-resection spontaneous metastasis experiments in *CnB*$^{fl/fl}$ (WT) and Col1a1-Cre-ER(T);*CnB*$^{fl/fl}$ (KO) mice. d, day. **D.** Volume of PDAC flank tumors on the indicated days prior to resection in the injection-resection experiment. **E.** Quantification of lung metastases (mets) per mouse and average size of lung mets. Size of lung mets was normalized to total lung area. N=13 (6 WT, 7 KO) each for LLC and PDAC experiments. **F.** Representative H&E images from PDAC and LLC lung metastases with fraction of metastasis-bearing mice indicated. Bar = 500 μm. Each slide represents all lung lobes from a single mouse. Error bar = standard deviation.